Effects of layer thickness and annealing process on low-frequency noise and detectivity in tunnel magnetoresistive sensors with CoFeSiB soft magnetic layers

Murali Krishnan Manikketh, Prabhanjan D. Kulkarni,* Tomoya Nakatani,** Hirofumi Suto, and Yuya Sakuraba

Research Center for Magnetic and Spintronic Materials, National Institute for Materials Science, 1-2-1, Sengen, Tsukuba, Ibaraki 305-0047, Japan,

* Present address: Centre for Sensors Vision Technology and IT, Central Manufacturing Technology Institute, Bengaluru, Karnataka, India.

** Corresponding author. Email: nakatani.tomoya@nims.go.jp

ABSTRACT

We investigated the effects of the CoFeSiB soft magnetic layer thickness and annealing process on the magnetic field sensing and low-frequency 1/*f* noise characteristics of tunnel magnetoresistive (TMR) sensors. A thicker CoFeSiB layer improved the soft magnetic properties of the free layer, and the process order of device fabrication and annealing significantly influenced the 1/*f* noise characteristics of the TMR sensors. A magnetic field detectivity of 0.8 nT/Hz$^{0.5}$ at 10 Hz was achieved in a single device TMR sensor annealed after the device fabrication, which suppressed both electrical and magnetic 1/*f* noise compared to the annealing performed before device fabrication. The spectral density of the 1/*f* noise voltage scaled linearly with the sensitivity of the sensor; thus, the detectivity showed an approximately constant value regardless of the change in sensitivity.

I. INTRODUCTION

Tunnel magnetoresistance (TMR) magnetic devices are promising for magnetic sensors in various fields owing to their high sensitivity, low power consumption, wide frequency response, small size, and room temperature operation advantages.[1–6] In particular, the development of TMR magnetometers for detecting very small magnetic fields is attracting considerable research attention, with promising applications in biomagnetic field sensing and nondestructive testing.[7–9] However, these applications require reduction of sensor noise at low frequencies, which is dominated by 1/*f* noise.[10,11] Previous studies have shown that the 1/*f* noise in TMR and giant magnetoresistive (GMR) sensors can be classified into two types of origin.[11–15] One is electrical 1/*f* noise, which is primarily due to lattice defects in the tunnel barrier. The other is magnetic 1/*f* noise, believed to be due to thermal fluctuations of the magnetization and magnetic domains.

The magnetic field-equivalent noise level of magnetic sensors, often referred to as the detectivity (*D*), is defined as

$$D = \sqrt{S_V}/(S \cdot V_\mathrm{b}), \tag{1}$$

where $\sqrt{S_V}$ is the spectral density of the noise voltage (unit: V/Hz$^{0.5}$), *S* is the sensitivity of the sensor defined by $\frac{1}{R} \cdot \frac{dR}{dH}$, and V_b is the bias voltage applied to the sensor. The power spectral density (S_V in V^2/Hz) of the 1/*f* noise in TMR devices is known to follow the empirical relationship of $S_V = \alpha_\mathrm{H} \frac{{V_\mathrm{b}}^2}{A} \frac{1}{f}$, where α_H is the Hooge's noise parameter representing the magnitude of the 1/*f* noise of the material system and *A* is the area of the tunnel barrier.[10] Therefore,

$$D = \sqrt{\alpha_\mathrm{H}}/(\sqrt{Af} \cdot S). \tag{2}$$

Note that α_H is correlated with *S*. Based on the fluctuation-dissipation theorem, α_H is expected to be linearly proportional to *S*.[12,13] From Eq. (2), an increase in *S* results in a decrease in *D*,

which is desirable for magnetic sensors. Although the scaling relationship of $\alpha_{\mathrm{H}} \propto S$ has been confirmed in experiments,[11,15–18] another type of scaling of $\alpha_{\mathrm{H}} \propto S^2$ has also been observed.[19–21] For $\alpha_{\mathrm{H}} \propto S^2$, from Eq. (2), D is independent of S. Therefore, an increase in S does not decrease D. The α_{H}-S scaling is thought to be governed by the magnetization process of the free layer (FL), the coherent magnetization rotation, or by the motion of magnetic domains.[15] However, a systematic study of the α_{H}-S dependence for highly sensitive TMR sensors is insufficient. Therefore, studying the α_{H}-S scaling in TMR and other spintronic magnetic sensor devices[22] is important from both practical and fundamental perspectives.

The soft magnetic properties of the FL are critical for magnetic sensors. The anisotropy field (H_{k}) of the FL determines S by $MR/2H_{\mathrm{k}}$, where MR is the magnetoresistance ratio. The coercivity (H_{c}) of the FL often leads to noise and error in magnetic field sensing. Although the CoFeB/MgO/CoFeB magnetic tunnel junctions[23,24] show large TMR ratios, the CoFeB FL does not exhibit sufficient soft magnetic properties for magnetic sensors because the amorphous CoFeB crystallizes to a bcc-CoFe with a relatively large H_{c}. Therefore, composite FL structures composed of a CoFeB layer and a soft magnetic layer have been widely used in TMR magnetic sensors. For example, NiFe/CoFeB and NiFe/Ru/CoFeB composite FLs have been developed.[25,26] However, the TMR ratio with these FLs tends to be lower than that with the CoFeB FL without NiFe. This is because the fcc-NiFe layer with the ⟨111⟩-oriented out-of-plane texture tends to degrade the crystallization of CoFeB into bcc-CoFe with the highly ⟨100⟩-oriented out-of-plane texture.[24] In subsequent studies, composite FLs with amorphous soft magnetic layers, such as CoFeSiB, CoFeBTa, and CoFeSiBTa, were developed with improved TMR ratios.[27–29] These amorphous soft magnetic materials are stable at 300–400 °C,[28–30] and the adjacent CoFeB layer does not receive a crystallization template effect from the amorphous soft magnetic layers.

To induce H_k in composite FLs and achieve magnetic sensor operation without an external bias magnetic field, the so-called *two-step annealing* process is often employed.[26,31] This process induces a magnetic easy axis of the FL that is orthogonal to the pinning direction of the pinned layer and the reference layer (RL). The thickness of the soft magnetic layer of the FL and the annealing process are known to significantly influence the TMR ratio and the magnetic properties of the FLs;[26–29,31,32] however, their effects on 1/*f* noise are not sufficiently understood, which is critical for developing TMR sensors with high sensitivity and low noise.

In this study, we investigated the effects of the thickness of CoFeSiB soft magnetic layers[27,33] and the two-step annealing conditions on the magnetic and noise properties of TMR sensors with a CoFeSiB/Ta/CoFeB composite FL. We found that the annealing temperature, and the device fabrication and annealing process order significantly affect the value of *D*. The difference in the 1/*f* noise properties of the TMR sensors with different CoFeSiB thicknesses and annealing conditions is discussed.

II. EXPERIMENTAL PROCEDURES

The TMR sensor stacks with the following layer structure were deposited by magnetron sputtering: thermally oxidized Si substrate/bottom electrode/Ta (5)/$Co_{70}Fe_5Si_{15}B_{10}$ (t_{CFSB})/Ta (0.3)/$Co_{40}Fe_{40}B_{20}$ (3)/MgO (1.8)/ $Co_{40}Fe_{40}B_{20}$ (2.5)/Ta (0.3)/ $Co_{40}Fe_{40}B_{20}$ (0.5)/ $Co_{50}Fe_{50}$ (1)/Ru (0.8)/ $Co_{50}Fe_{50}$ (3)/ $Ir_{20}Mn_{80}$ (8)/Ru (8) (thickness in nm and alloy composition in at. %), as shown in Fig. 1(a). The bottom electrode comprised a Ta (5)/Cu (100)/Ta (10)/Ru (10) structure, and the surface of the Ta (10) layer was planarized via chemical mechanical polishing. Devices with four different CoFeSiB FL thicknesses [t_{CFSB}(nm) = 10, 20, 40, and 80] were fabricated. The films were patterned using optical lithography and Ar ion milling. MTJ pillars with 60-μm diameters were milled down to the surface of the FL. The FL was patterned to a rectangular shape of 440×180 μm.

As shown in Fig. 1(b), we performed a two-step annealing process either before or after device fabrication process. This paper refers to the annealing process performed before device fabrication as *pre-fabrication annealing* and that performed after device fabrication as *post-fabrication annealing*. In both cases, the first annealing was performed at T_1 = 350 °C for 1 h under an external magnetic field of 0.7 T in the +*x* direction. A subsequent second annealing was performed for 1 h at T_2 = 180−250 °C under 0.7 T in the +*y* direction. T_2 for the pre- and post-fabrication annealing are referred to as T_2^{pre} and T_2^{post}, respectively. The first annealing induces uniaxial magnetic anisotropy along the FL in the *x*-axis, and the second annealing pins the magnetization of the CoFe pinned layer next to the IrMn antiferromagnetic layer in the +*y* direction. The magnetization of the RL is pinned in the −*y* direction owing to the antiferromagnetic interlayer exchange coupling through the Ru (0.8 nm) layer. Consequently, the FL magnetization is stabilized in the direction orthogonal to that of the RL, technically termed as *crossed anisotropy,* and the TMR device obtains a sensitivity axis on the *y*-axis.

The *R*-*H* curves and noise characteristics of the TMR devices were measured in a triple-walled permalloy magnetic shielding box using the DC four-probe technique. An external magnetic field (*H*) was applied along the magnetic hard axis of the FL (*y*-axis). Figure 2 shows the circuit diagram for the noise measurement. Bias voltage (V_{b}) was applied to a TMR device using a 1.5 V dry cell. By adjusting the resistance of the ballast resistor (potentiometer), the bias voltage across the TMR device was set to V_{b0} = 30 mV at H = 0. This supplies an approximately constant bias current to the device. When H is applied, the device resistance, R, changes; therefore, V_{b} follows $V_{\mathrm{b}} = R(H)/R_{H=0} \cdot V_{\mathrm{b0}}$. The noise across the TMR device was amplified to 40 dB using a low-noise preamplifier (NF Corporation, SA-200F3) and recorded using a 24-bit digitizer (NI, PCI-4461).

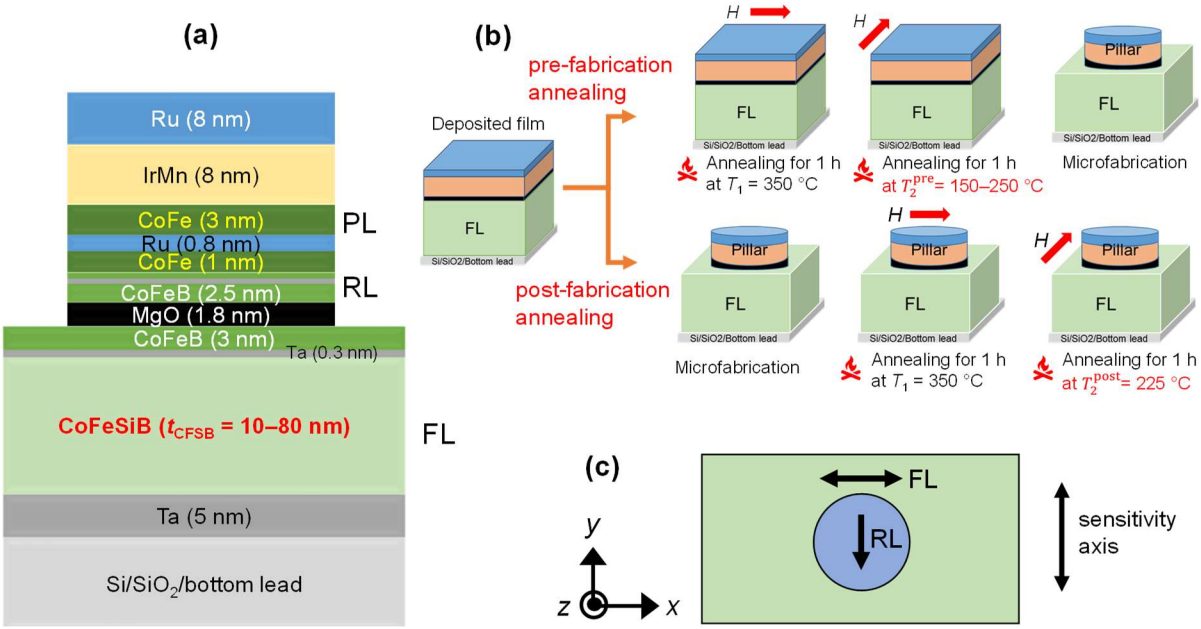

FIG. 1. Schematics of (a) layer structure, (b) annealing process, and (c) top view of the TMR device and the magnetization easy axis of the reference layer (RL) and free layer (FL).

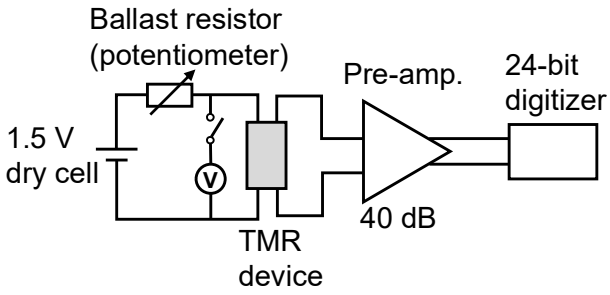

FIG. 2. Circuit diagram for the noise measurement.

III. RESULTS

A. Second annealing temperature dependence

First, we investigated the effect of the second annealing temperature of the pre-fabrication annealing process (T_2^{pre}) for the devices with t_{CFSB} = 20 nm. Figure 3(a) shows the magnetization–magnetic field (M–H) curves of the unpatterned TMR films annealed at different T_2^{pre}. The plateau of the M–H curve observed between $\mu_0 H = 0$ mT and ~40 mT for T_2^{pre} = 180–

250 °C corresponds to the antiparallel (AP) magnetization state between the FL and RL. The kink in the *M–H* curve at $\mu_0 H$ ~40 mT indicates the effective pinning field for the RL. The film for T_2^{pre} = 150 °C did not show a clear AP magnetization state, indicating insufficient exchange bias pinning for the RL. Figure 3(b) shows the TMR ($\Delta R/R_{\mathrm{min}}$) curves of the devices. The resistance–magnetic field (*R–H*) curves are shown in Fig. S1 in the supplementary material. The resistance-area product values in the P-state (RA_{P}) were in the 25–120 kΩ μm^2 range depending on T_2^{pre} with a trend of increased RA_{P} at $T_2^{\mathrm{pre}} \geq 225$ °C. For T_2^{pre} = 150 °C, the TMR ratio was only ~88% owing to insufficient pinning, which was also evident from the increase in *R* as *H* became more negative, indicating RL magnetization rotation. The TMR ratios were >160% for $T_2^{\mathrm{pre}} \geq$ 180 °C, indicating that $T_2^{\mathrm{pre}} \geq$180 °C was required to obtain a sufficient pinning of the RL and a high TMR ratio. The TMR curves in Fig. 3(b) show a gradual change in the resistance between the parallel (P) and AP magnetization states because of the crossed anisotropy induced by the two-step annealing process. The anisotropy field (H_{k}) of the FL was defined as ($H_{95\%}$–$H_{5\%}$)/2, where $H_{95\%}$ and $H_{5\%}$ are the magnetic fields at which $\Delta R/R_{\mathrm{min}}$ reached the 95% and 5% of the maximum value, respectively. H_{k} exhibited systematic decrease as T_2^{pre} increased, as shown in Fig. 3(c). This leads to an increase in the magnetic field sensitivity (*S*) of the TMR sensor at higher T_2^{pre}. However, the devices with T_2^{pre} = 225 and 250 °C showed large hysteresis. Similar behaviors of decreasing H_{k} and increasing hysteresis with increased T_2 were also observed for CoFeBTa/Ta/CoFeB composite FLs, and their origins were explained by additional magnetic anisotropy in the FL induced by the second annealing process.[28]

Figures 3(d) and (e) show the noise spectra of the TMR devices in the P magnetization state ($\mu_0 H$ = −3 mT) and the intermediate magnetization state with the highest *S* (e.g., at $\mu_0 H$ = 1.0 and 0.6 mT for T_2^{pre} = 180 and 250 °C, respectively). Because these devices exhibited magnetic hysteresis, we first saturated the magnetization configuration in the AP state and

reduced H to achieve the intermediate state. In both the P and intermediate states, all the devices exhibited 1/f noise spectra, which is typical for TMR devices. However, the magnitude of the 1/f noise in the intermediate magnetization state was much larger than that in the P state owing to the 1/f noise with magnetic origin. This resulted in a significant increase in the corner frequency of the 1/f noise, defined as the frequency at which the 1/f noise spectral density becomes equal to the thermal white noise, from the order of 10^3 Hz in the P state to the order of 10^4 Hz in the intermediate state. Figure 3(f) shows the spectra of D in the intermediate state, showing comparable values of D at low frequencies for the devices annealed at T_2^{pre} = 180–250 °C.

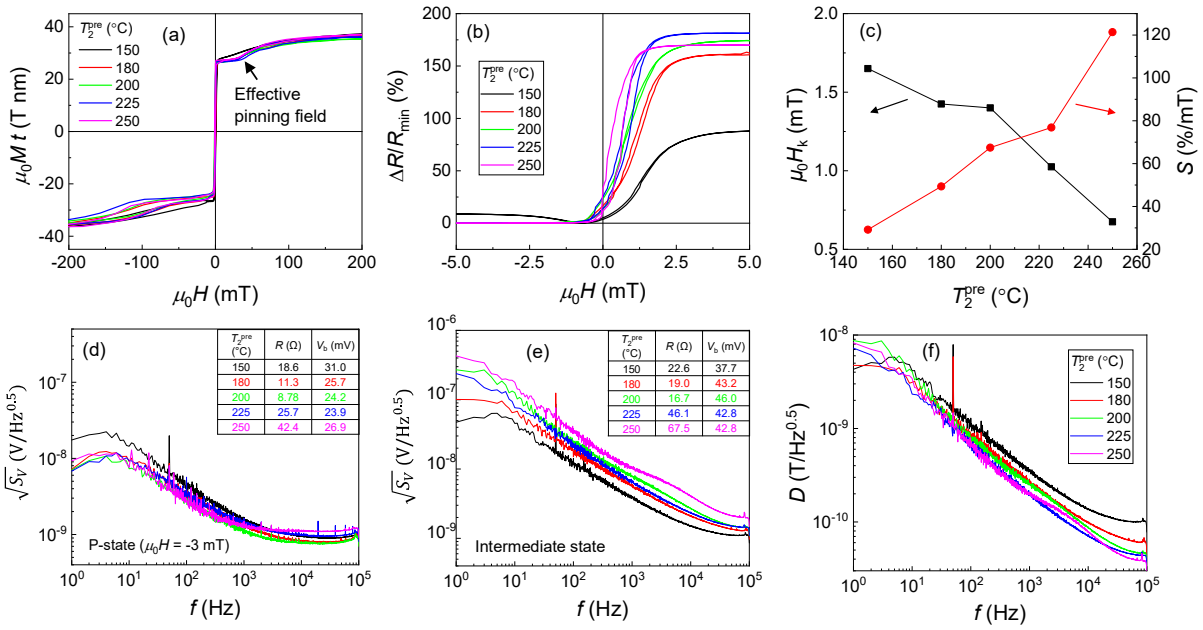

FIG. 3. (a) M–H and (b) $\Delta R/R_{\mathrm{min}}$–$H$ curves of the TMR devices with t_{CFSB} = 20 nm processed at different second pre-fabrication annealing temperatures (T_2^{pre}). (c) T_2^{pre} dependence of the anisotropy field (H_{k}) and sensitivity (S). (d) Noise spectra in the parallel magnetization state at $\mu_0 H$ = −3 mT. Spectra of (e) noise and (f) detectivity in the intermediate magnetization states

with the highest *S*. For (d)–(f), the roll-off below 5 Hz was caused by the cutoff of the AC input of the analyzer, and the peaks observed above 10 kHz were caused by external noise.

B. CoFeSiB thickness dependence

Next, the dependence of the sensitivity, noise, and detectivity on t_{CFSB} was investigated. For the devices with t_{CFSB} = 20 nm, T_2^{pre} = 180 °C provided sufficient pinning, a high TMR ratio of 160%, a small coercivity, and the lowest noise, as shown in Fig. 3. Thus, we used T_2^{pre} = 180 °C for the t_{CFSB} dependence study. The device with t_{CFSB} = 10 nm showed RA_P = 78.6 kΩ μm^2, and those with t_{CFSB} = 20–80 nm showed similar values of RA_P of ~35 kΩ μm^2 (see the supplementary material.). Figure 4(a) shows the TMR curves for t_{CFSB} = 10–80 nm. The TMR ratio for t_{CFSB} = 10 nm (134%) was significantly lower than those for t_{CFSB} = 20–80 nm (~155%). In addition, the magnetic hysteresis for t_{CFSB} = 10 nm was much larger than those for the other values of t_{CFSB}. The device with t_{CFSB} = 80 nm exhibited the best soft magnetic properties in terms of small hysteresis and H_k, resulting in the highest *S* of 93.4 %/mT as shown in Fig. 4(b). The improvements in the soft magnetic properties and *S* for thicker FLs are consistent with previous reports on NiFe-based[26,31] and CoFeSiB-based[27] composite FLs.

Figure 4(c) shows the noise spectra of the TMR devices with different t_{CFSB} values under a constant bias magnetic field of +1 mT. The devices all showed similar 1/*f* noise levels despite the large variation of *S*; $\sqrt{S_V}$ = 81.4 and 96.1 nV/Hz$^{0.5}$ at 10 Hz, and *S* = 49.3 and 93.4 %/mT for t_{CFSB} = 20 and 80 nm, respectively, as shown in Figs. 4(b) and 4(d). A minimum value of *D* at 10 Hz of 2.1 nT/Hz$^{0.5}$ was obtained for t_{CFSB} = 80 nm.

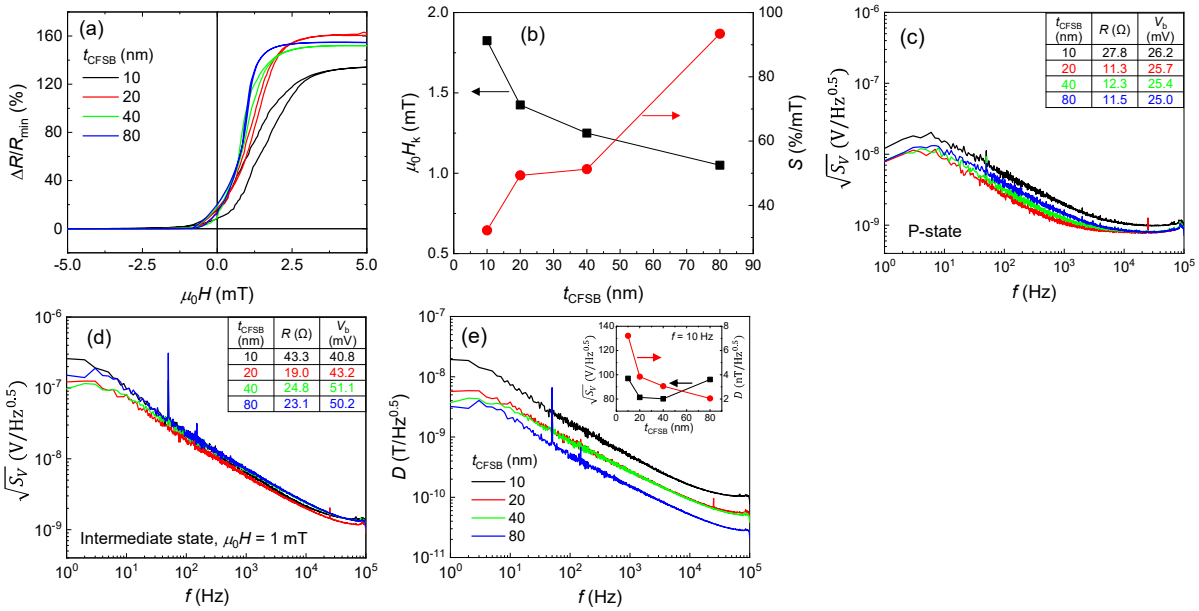

t_{CFSB} (nm)	R (Ω)	V_b (mV)
10	27.8	26.2
20	11.3	25.7
40	12.3	25.4
80	11.5	25.0

t_{CFSB} (nm)	R (Ω)	V_b (mV)
10	43.3	40.8
20	19.0	43.2
40	24.8	51.1
80	23.1	50.2

FIG. 4. (a) $\Delta R/R_{min}$–H curves of the devices with t_{CFSB} = 20–80 nm and T_2^{pre} = 180 °C. (b) The t_{CFSB} dependences of H_k and S. Noise voltage spectral densities in the (c) P-state and (d) intermediate state. Spectral densities of the (d) noise voltage and (e) detectivity in the intermediate states. The inset in (e) shows the t_{CFSB} dependencies of the spectral densities of the voltage density and detectivity at f = 10 Hz.

C. Effect of post-fabrication annealing

To discuss the effect of the process order of the device fabrication and annealing on the TMR and the noise properties, we compared the properties of the TMR devices for t_{CFSB} = 80 nm with pre-fabrication annealing at T_2^{pre} = 180 and 225 °C and post-fabrication annealing at T_2^{post} = 225 °C, as shown in Fig. 5(a). Compared to the device for T_2^{pre} = 180 °C, the device for T_2^{pre} = 225 °C showed a higher TMR ratio and a lower H_k, resulting in a maximum S of 164 %/mT, which is consistent with the results for t_{CFSB} = 20 nm (Fig. 3(b)). However, unlike in the case of t_{CFSB} = 20 nm, a higher T_2^{pre} did not significantly increase the hysteresis of the TMR curve for t_{CFSB} = 80 nm because of the improved magnetic softness of the thicker CoFeSiB film. The TMR ratio and S were further enhanced to 209% and 168 %/mT, respectively, by post-

fabrication annealing at T_2^{post} = 225 °C. The values of RA_{P} were 32.5, 45.1, and 7.2 kΩ μm^2 for T_2^{pre} = 180 and 225 °C and T_2^{post} = 225 °C, respectively, (see the supplementary material).

Figures 5(b) and (c) show the noise spectra of the devices in the P and intermediate magnetization states, respectively. In the P state, the device with T_2^{post} = 225 °C showed a significantly reduced 1/f noise compared to those with T_2^{pre} = 180 and 225 °C. The corresponding α_{H} values were 1.7×10^{-10} μm^2 for T_2^{post} = 225 °C, and 5.6×10^{-9} and 4.4×10^{-9} μm^2 for T_2^{pre} = 180 and 225 °C, respectively. Because the 1/f noise observed in the P state is considered to be of purely electrical origin, the suppressed 1/f noise for T_2^{post} = 225 °C may be due to reduced lattice defects in the MgO barrier or at the CoFeB/MgO interface. The post-fabrication annealing process may recover lattice defects, such as those induced during Ar ion milling. In the intermediate magnetization state, as shown in Fig. 5(c), the device processed at T_2^{post} = 225 °C showed a lower 1/f noise than the other devices. The corresponding α_{H} values for T_2^{post} = 225 °C, T_2^{pre} = 180 and 225 °C, were 3.5×10^{-8}, 1.7×10^{-7}, and 1.1×10^{-7} μm^2, respectively.

Figure 5(d) shows the magnetic field dependence of α_{H} of these devices. The device for T_2^{post} = 225 °C showed a lower α_{H} compared to the other devices in the P state and in the intermediate magnetization state. The variations in the magnetic 1/f noise of these three devices are discussed in Sec. IV. Figure 5(e) shows the magnetic field dependence of D at f = 10 Hz. D was calculated with the values of $\sqrt{S_V}$, S from the TMR curve, and V_{b} at each value of H. Interestingly, in the intermediate magnetization state (−0.6 mT ≤ H ≤ +0.8 mT), where the devices exhibited non-zero S, D showed an approximately constant value for each device: D = 2.6±0.5, 1.7±0.5, and 0.8±0.2 nT/Hz$^{0.5}$ at f = 10 Hz for T_2^{pre} = 180 and 225 °C, and T_2^{post} = 225 °C, respectively.

We plotted the noise voltage density $\sqrt{S_V}$, for sensitivity in terms of $\frac{dR}{dH}$ in Fig. 5(f) to understand this behavior. The reason for plotting $\sqrt{S_V}$ versus $\frac{dR}{dH}$ instead of the commonly used sensitivity defined by $S = \frac{dR}{dH} \cdot \frac{1}{R}$ is as follows. As mentioned in II. EXPERIMENTAL PROCEDURES, V_b is H-dependent in our noise measurement, following $V_\mathrm{b} = R(H)/R_{H=0} \cdot V_{\mathrm{b}0}$. Therefore, from Eq. (1), $D = \sqrt{S_V}/(\frac{dR}{dH} \cdot \frac{V_{\mathrm{b}0}}{R_{H=0}})$, indicating that the $\sqrt{S_V}$–$\frac{dR}{dH}$ relationship determines the H-dependence of D. As shown in Fig. 5(f), $\sqrt{S_V}$ scales linearly with $\frac{dR}{dH}$, therefore, D showed approximately constant values in the intermediate magnetization state, despite the change in sensitivity. Note that such a linear scaling relationship between $\sqrt{S_V}$ and $\frac{dR}{dH}$ or S has been observed experimentally in TMR devices.[19–21]

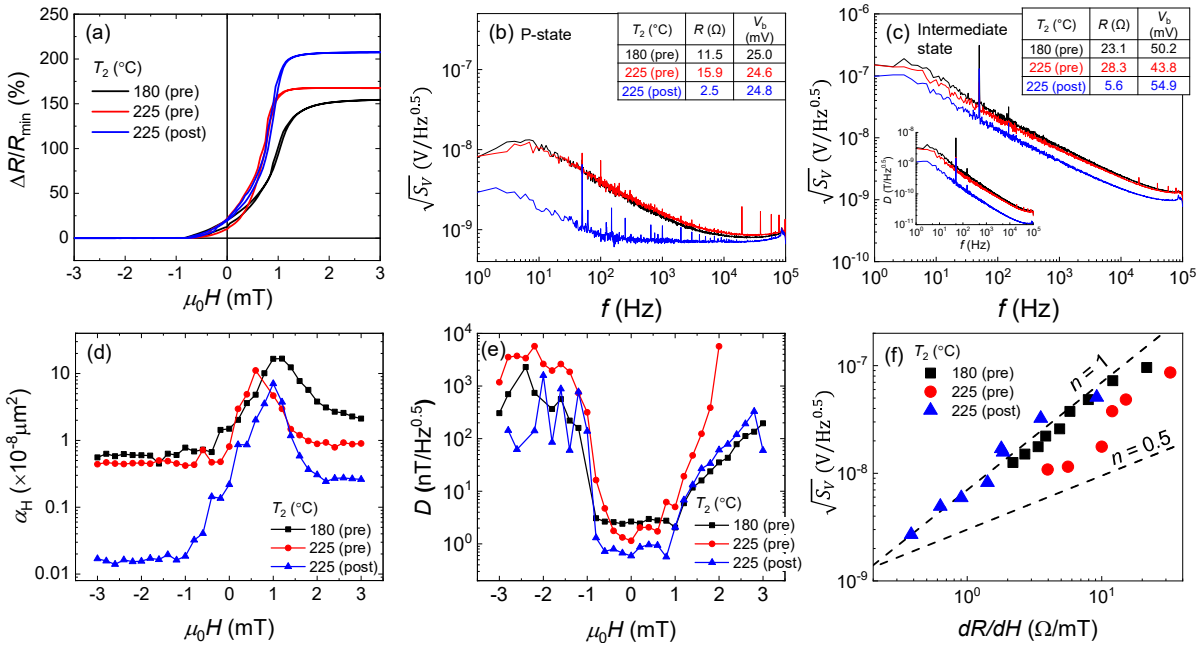

FIG. 5. (a) $\Delta R/R_{\mathrm{min}}$–$H$ curves and noise voltage ($\sqrt{S_V}$) spectra in (b) the P state and (c) the intermediate magnetization state of the devices with different T_2 conditions. The inset in (c) shows the detectivity spectra in the intermediate state. Magnetic field dependence of (d) Hooge's noise parameter (α_H) and (e) D at f = 10 Hz. (f) Dependence of $\sqrt{S_V}$ at f = 10 Hz on

$\frac{dR}{dH}$. The dashed lines show $\sqrt{S_V} = a\left(\frac{dR}{dH}\right)^n$, where a is a constant and n = 0.5 and 1. t_{CFSB} = 80 nm for all devices

Table 1 summarizes the properties of the present and previously reported TMR sensor devices with different FL materials. Because $\sqrt{S_V}$ and D are inversely proportional to $\sqrt{A}$ (Eq. (2)), α_H and $\sqrt{A} \cdot D$ are the appropriate parameters to compare the magnitude of 1/f noise and D, respectively, of the TMR devices with different A. Compared with the TMR device with the amorphous CoFeBTa-based FL,[28] the present device with the CoFeSiB-based FL exhibited improved S and comparable α_H, resulting in a smaller $\sqrt{A} \cdot D$. Using a 150-nm-thick CoFeSiB-based FL, Oogane *et al*.[8] reported D ~0.03 nT/Hz$^{0.5}$ at 10 Hz for a TMR sensor comprising 74 MTJs connected in series. The corresponding $\sqrt{A} \cdot D$ of 13 μm·nT/Hz$^{0.5}$ is the lowest value ever reported. They achieved D < 0.3 pT/Hz$^{0.5}$ at 10 Hz using magnetic flux concentrators.

Table 1. Comparison of the properties of the reported and present TMR sensor devices with NiFe, CoFeBTa, and CoFeSiB soft magnetic layers.

	Ref [34]	Ref [28]	Ref [8]	Ref [33]	Present study
FL material	NiFe	CoFeBTa	CoFeSiB		
T_2 (°C)	300	200	225	250	225
FL thickness (nm)	70	20	140	30	80
Device structure	single device	single device	74 MTJs array	single device	single device
MTJ area, A (μm^2)	3,200	1,962	185,000	300	2,826
TMR ratio (%)	140	155	>200	200	209
H_k (mT)	0.3	1.2	0.1	1.63	1.1
S (%/mT)	250	70	1150	n/a	168

			single MTJ		
$\sqrt{S_V}$ at 10 Hz (V/Hz$^{0.5}$)	n/a	4.6×10^{-8}	n/a	4.3×10^{-8}	5.1×10^{-8}
α_H (μm^2)	3.3×10^{-7} P-state	4×10^{-8}	1.2×10^{-9} P-state	4×10^{-9}	3.5×10^{-8}
D at 10 Hz (nT/Hz$^{0.5}$)	n/a	2.2	~0.03	4.5	0.8
$\sqrt{A} \cdot D$ (μm·nT/Hz$^{0.5}$)	n/a	97	~13	78	43

IV. DISCUSSION

This section discusses the variations in the magnetic 1/*f* noise in the three devices with t_{CFSB} = 80 nm and the different annealing processes described in Sec. III. C. As shown in Figs. 5(b) and (d), the device with T_2^{post} = 225 °C exhibited significantly reduced electrical 1/*f* noise in the P state compared with the other devices processed with pre-fabrication annealing. In the intermediate magnetization state with high *S*, all devices exhibited a higher 1/*f* noise than those in the P state. However, the device with T_2^{post} = 225 °C again showed a lower 1/*f* noise than the other devices. Electrical and magnetic 1/*f* noises are generally assumed to be independent,[14] and the power spectrum of 1/*f* noise is expressed as the sum of those of the electrical and magnetic 1/*f* noise: $S_V = S_V^{ele} + S_V^{mag}$. Similarly, $\alpha_H = \alpha_H^{ele} + \alpha_H^{mag}$. Figure 6(a) shows the $\sqrt{S_V^{mag}}$ spectra of the devices obtained by subtracting S_V^{ele} measured in the P state (Fig. 5(b)) from S_V in the intermediate state (Fig. 5(d)). The device with T_2^{post} = 225 °C showed a lower $\sqrt{S_V^{mag}}$ spectrum. In the fluctuation-dissipation theorem, assuming a uniform FL magnetization in thermal equilibrium,[13,15] the Hooge's parameter of the magnetic 1/*f* noise, α_H^{mag}, is expressed as

$$\alpha_H^{mag} = \varepsilon(f,H)\frac{k_B T}{\pi\mu_0 M_S}\frac{\Delta R}{R}\left(\frac{1}{R}\frac{dR}{dH}\right), \quad (3)$$

where $\varepsilon(f,H)$ is the phase lag of the resistance response to an AC magnetic field ($\varepsilon(f,H) \equiv \chi_R^{''}/\chi_R'$), $\chi_R^{''}$ and χ_R' are the imaginary and real parts of the resistance susceptibility, respectively, k_B is the Boltzmann constant, T is the temperature, μ_0 is the vacuum permeability, M_s is the saturation magnetization, and $\Delta R = R_{AP} - R_P$. Note that $\frac{\Delta R}{R}$ is not the full TMR ratio (= $\Delta R/R_P$) but is ΔR divided by R at each sensor operating point. $\frac{\Delta R}{R}\left(\frac{1}{R}\frac{dR}{dH}\right)$ is called the magnetoresistance-sensitivity product (MSP).

Figure 6(b) shows the α_H vs. MSP of the three devices from the P state to the maximum MSP, showing nonlinear curves despite the linear dependence of α_H^{mag} on MSP by Eq. (3). For all types of devices, α_H showed approximately constant values below the threshold values of MSP, e.g., MSP ~0.3, 0.7, and 0.8 mT^{-1} for T_2^{pre} = 180, 225 °C, and T_2^{post} = 225 °C, respectively. Above the threshold values of MSP, α_H increased significantly with increasing MSP. Figures 6(c) and (d) show the H dependence of MSP and α_H of T_2^{pre} = 180 °C and T_2^{post} = 225 °C devices, respectively. The R-H curves are shown in the insets. The shaded regions indicate the states showing a large increase in α_H when MSP is increased. Both devices showed non-zero S and MSP at approximately H = 0, where the α_H values were close to those in the P states. A rapid increase in α_H was observed as S and MSP increased. The nonlinear α_H–MSP curves of the present TMR devices suggest that the magnetic 1/f noise is not only due to the thermal fluctuation of uniform magnetization, which is expressed by Eq. (3). Note that the FL with uniaxial magnetic anisotropy is demagnetized with the multi-domain structure under zero H. Therefore, when an external H is applied to the hard axis, the FL is magnetized through a magnetic domain wall motion, and the magnetization is saturated at above H_k. Therefore, the large increase in α_H in the high-S state may be related to the motion of magnetic domain walls and their pinning and depinning at defect sites, i.e., Barkhausen-type domain motion.

We also analyzed the H dependences of H_c in the R–H curves of the three devices with variations in the annealing condition, as shown in Fig. S2 in the supplementary materials. The largest 1/f noise was observed at $\mu_0 H$ ~1 mT for all the devices, where the values of H_c were relatively small. Therefore, we observed no clear correlation between H_c and the magnetic 1/f noise. In addition, we measured the phase lag for the devices with T_2^{pre} = 225 °C, and T_2^{post} = 225 °C; however, we did not observe a clear difference in the phase lag values between these two devices.

These results demonstrate that post-fabrication annealing increases the TMR ratio and S and decreases both the electrical and magnetic 1/f noises, which is significantly beneficial for the development of TMR sensors with fine magnetic field resolutions. The increased TMR ratio and decreased electrical 1/f noise may be related to the recovery of lattice defects by post-fabrication annealing, such as those caused by the Ar ion milling during device fabrication. We also conducted experimental investigations to understand the relationship between reduced magnetic 1/f noise and improved soft magnetic properties obtained by post-fabrication annealing, such as the magnetic damping of the patterned FLs. However, no reasonable correlation has been observed. Therefore, further studies are required to understand the mechanism of the suppressed magnetic 1/f noise due to post-fabrication annealing.

Furthermore, to deepen the understanding of the mechanism that determines the scaling between noise spectral density and sensitivity (or MSP), investigations of the noise properties in TMR devices with different soft magnetic materials and/or different methods of the FL magnetization stabilization, such as by the soft-pinning by exchange bias[18,25,35] and external magnetic field, are important.

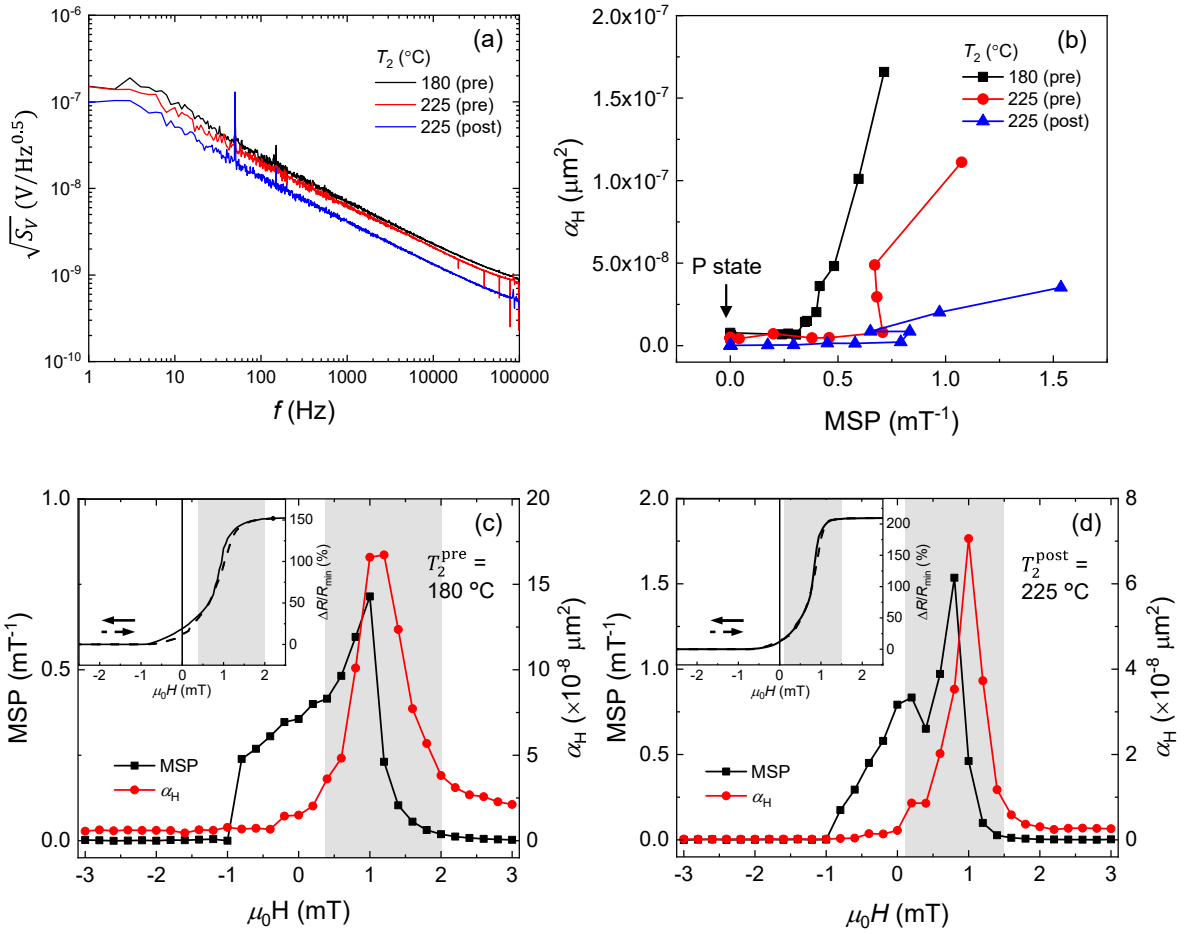

FIG. 6. (a) Spectra of the magnetic 1/*f* noise at the highest *S* states for the devices annealed at T_2^{pre} = 180 and 225 °C, and T_2^{post}= 225 °C. (b) α_{H} vs. magnetoresistance-sensitivity product (MSP). Magnetic field dependence of the α_{H} and MSP of the devices annealed at (c) T_2^{pre} = 180 °C and (d) T_2^{post}= 225 °C. The insets in (c) and (d) are the $\Delta R/R_{\mathrm{min}}$–$H$ curves of the devices.

V. CONCLUSIONS

The TMR and 1/*f* noise characteristics of CoFeB/MgO/CoFeB-MTJ-based sensor devices using a composite FL with an amorphous CoFeSiB soft magnetic layer were investigated. A two-step annealing process at temperatures of T_1 = 350 °C and T_2 = 180–250 °C was employed to obtain a uniaxial magnetic anisotropy of FL and an *R*-*H* response with low coercivity. Consistent with previous studies, the soft magnetic properties of the CoFeSiB-based

composite FL improved with thickness, and we obtained a high sensitivity of up to 168 %/mT ($\Delta R/R_{min}$ = 209% and H_k = 1.1 mT) by using an 80-nm-thick CoFeSiB and optimizing the annealing condition. This sensor with an MTJ area of 2,826 μm^2 achieved a magnetic field detectivity of D = 0.8 nT/Hz$^{0.5}$ at f = 10 Hz, which is the lowest value ever reported for a single TMR device without magnetic flux concentrators. We found that the annealing process performed after device fabrication (post-fabrication annealing) significantly improved the TMR ratio and decreased both the electrical and magnetic 1/f noises, which is beneficial for the development of TMR sensors with ultra-fine D. However, the mechanism for 1/f noise reduction is an open question. In addition, the magnetic 1/f noise voltage density scales linearly with sensitivity. Therefore, D has an approximately constant value in the intermediate magnetization state, despite the sensitivity variation.

Acknowledgements

This work was partly supported by JSPS KAKENHI (Grant No. 24K00932).

Supplementary material

See the supplementary material for additional data on the R-H curves, H_c, and resistance susceptibility including the phase lag.

Author Declarations

The authors have no conflicts to disclose.

Data Availability Statement

The data supporting the findings of this study are available from the corresponding author upon reasonable request

References

[1] M. Tondra, J.M. Daughton, D. Wang, R.S. Beech, A. Fink, and J.A. Taylor, J. Appl. Phys. **83**, 6688 (1998).

[2] P.P. Freitas, R. Ferreira, S. Cardoso, and F. Cardoso, J. Phys. Condens. Matter **19**, 165221 (2007).

[3] R.C. Chaves, P.P. Freitas, B. Ocker, and W. Maass, Appl. Phys. Lett. **91**, 102504 (2007).

[4] S.H. Liou, X. Yin, S.E. Russek, R. Heindl, F.C.S. Da Silva, J. Moreland, D.P. Pappas, L. Yuan, and J. Shen, IEEE Trans. Magn. **47**, 3740 (2011).

[5] S. Cardoso, D.C. Leitao, T.M. Dias, J. Valadeiro, M.D. Silva, A. Chicharo, V. Silverio, J. Gaspar, and P.P. Freitas, J. Phys. D. Appl. Phys. **50**, 213001 (2017).

[6] D. Suess, A. Bachleitner-Hofmann, A. Satz, H. Weitensfelder, C. Vogler, F. Bruckner, C. Abert, K. Prügl, J. Zimmer, C. Huber, S. Luber, W. Raberg, T. Schrefl, and H. Brückl, Nat. Electron. 2018 16 **1**, 362 (2018).

[7] K. Fujiwara, M. Oogane, A. Kanno, M. Imada, J. Jono, T. Terauchi, T. Okuno, Y. Aritomi, M. Morikawa, M. Tsuchida, N. Nakasato, and Y. Ando, Appl. Phys. Express **11**, 023001 (2018).

[8] M. Oogane, K. Fujiwara, A. Kanno, T. Nakano, H. Wagatsuma, T. Arimoto, S. Mizukami, S. Kumagai, H. Matsuzaki, N. Nakasato, and Y. Ando, Appl. Phys. Express **14**, 123002 (2021).

[9] A. Kanno, N. Nakasato, M. Oogane, K. Fujiwara, T. Nakano, T. Arimoto, H. Matsuzaki, and Y. Ando, Sci. Rep. **12**, 6106 (2022).

[10] E.R. Nowak, M.B. Weissman, and S.S.P. Parkin, Appl. Phys. Lett. **74**, 600 (1999).

[11] S. Ingvarsson, G. Xiao, S.S.P. Parkin, W.J. Gallagher, G. Grinstein, and R.H. Koch, Phys. Rev. Lett. **85**, 3289 (2000).

[12] H.T. Hardner, M.B. Weissman, M.B. Salamon, and S.S.P. Parkin, Phys. Rev. B **48**, 16156

(1993).

[13] N. Smith, A.M. Zeltser, D.L. Yang, and P. V. Koeppe, IEEE Trans. Magn. **33**, 3385 (1997).

[14] W.F. Egelhoff, P.W.T. Pong, J. Unguris, R.D. McMichael, E.R. Nowak, A.S. Edelstein, J.E. Burnette, and G.A. Fischer, Sensors Actuators A Phys. **155**, 217 (2009).

[15] A. Ozbay, A. Gokce, T. Flanagan, R.A. Stearrett, E.R. Nowak, and C. Nordman, Appl. Phys. Lett. **94**, 202506 (2009).

[16] L. Jiang, E.R. Nowak, P.E. Scott, J. Johnson, J.M. Slaughter, J.J. Sun, and R.W. Dave, Phys. Rev. B **69**, 054407 (2004).

[17] Z. Diao, E.R. Nowak, K.M. Haughey, and J.M.D. Coey, Phys. Rev. B **84**, 094412 (2011).

[18] J.Y. Chen, J.F. Feng, and J.M.D. Coey, Appl. Phys. Lett. **100**, 142407 (2012).

[19] C. Ren, X. Liu, B.D. Schrag, and G. Xiao, Phys. Rev. B **69**, 104405 (2004).

[20] D. Mazumdar, X. Liu, B.D. Schrag, M. Carter, W. Shen, and G. Xiao, Appl. Phys. Lett. **91**, 033507 (2007).

[21] W. Zhang, Q. Hao, and G. Xiao, Phys. Rev. B **84**, 094446 (2011).

[22] Y. Zhang, K. Wang, and G. Xiao, Appl. Phys. Lett. **116**, 212404 (2020).

[23] D.D. Djayaprawira, K. Tsunekawa, M. Nagai, H. Maehara, S. Yamagata, N. Watanabe, S. Yuasa, Y. Suzuki, and K. Ando, Appl. Phys. Lett. **86**, 092502 (2005).

[24] S. Yuasa and D.D. Djayaprawira, J. Phys. D. Appl. Phys. **40**, R337 (2007).

[25] R. Ferreira, E. Paz, P.P. Freitas, J. Wang, and S. Xue, IEEE Trans. Magn. **48**, 3719 (2012).

[26] K. Fujiwara, M. Oogane, S. Yokota, T. Nishikawa, H. Naganuma, and Y. Ando, J. Appl. Phys. **111**, 07C710 (2012).

[27] D. Kato, M. Oogane, K. Fujiwara, T. Nishikawa, H. Naganuma, and Y. Ando, Appl. Phys. Express **6**, 103004 (2013).

[28] M. Rasly, T. Nakatani, J. Li, H. Sepehri-Amin, H. Sukegawa, and Y. Sakuraba, J. Phys. D. Appl. Phys. **54**, 095002 (2021).

[29] T. Nakano, K. Fujiwara, M. Tsunoda, S. Kumagai, and M. Oogane, Appl. Phys. Lett. **123**, 72404 (2023).

[30] Y.S. Choi, T. Nakatani, J.C. Read, M.J. Carey, D.A. Stewart, and J.R. Childress, Appl. Phys. Express **10**, 013006 (2017).

[31] K. Fujiwara, M. Oogane, F. Kou, D. Watanabe, H. Naganuma, and Y. Ando, Jpn. J. Appl. Phys. **50**, 013001 (2011).

[32] S.H. Liou, R. Zhang, S.E. Russek, L. Yuan, S.T. Halloran, and D.P. Pappas, J. Appl. Phys. **103**, 07E920 (2008).

[33] L. Huang, Z.H. Yuan, B.S. Tao, C.H. Wan, P. Guo, Q.T. Zhang, L. Yin, J.F. Feng, T. Nakano, H. Naganuma, H.F. Liu, Y. Yan, and X.F. Han, J. Appl. Phys. **122**, 113903 (2017).

[34] K. Fujiwara, M. Oogane, T. Nishikawa, H. Naganuma, and Y. Ando, Jpn. J. Appl. Phys. **52**, 04CM07 (2013).

[35] D. Wang, J. Daughton, C. Nordman, P. Eames, and J. Fink, J. Appl. Phys. **99**, 08H703 (2006).